Heterogeneous mass loss of glaciers in the Aksu-Tarim Catchment (Central Tien Shan) revealed by 1976 KH-9 Hexagon and 2009 SPOT-5 stereo imagery

Pieczonka, Tino ; Bolch, Tobias ; Junfeng, Wei ; Shiyin, Liu

Abstract: The meltwater released by the glaciers in the Aksu-Tarim Catchment, south of Tomur Peak (Central Tien Shan), feeds the Tarim River which is the main artery for the oases at the northern margin of the Taklamakan desert. The correct modeling of the contribution of the glaciers meltwater to the total runoff of the Tarim River is hampered by the lack of mass balance data. Multi-temporal digital terrain models (DTMs) allow the determination of volume changes for large samples of glacier. Here, we present the mass changes for 12 glaciers using 1976 KH-9 Hexagon, 2000 SRTM3 and 2009 SPOT-5 datasets. The results show that most of the glaciers have been losing mass since 1976. The largest glaciers, Koxkar and West Qongterang, lost !0.27±0.15 m w.e.a ^{1} and !0.43±0.15 m w.e.a ^{1} between 1976 and 2009, despite thick debris cover. However, some smaller glaciers show mass gain at their tongues indicating glacier surges. Using SRTM3 data the volume gain of Qinbingtan Glacier No. 74 could be dated to the time period 1999–2009. The overall mass budget of ! 0.33 ± 0.15 m w.e.a ^{1} (for 1976–2009) of the investigated glaciers is within the variability range of the global average. However, in the recent years (1999–2009) a slightly decelerated mass loss of !0.23±0.19 m w.e.a ^{1} could be observed.

DOI: https://doi.org/10.1016/j.rse.2012.11.020

(This is a sample cover image for this issue. The actual cover is not yet available at this time.)

Remote Sensing of Environment 130 (2013) 233–244

Contents lists available at SciVerse ScienceDirect

Remote Sensing of Environment

journal homepage: www.elsevier.com/locate/rse

Heterogeneous mass loss of glaciers in the Aksu-Tarim Catchment (Central Tien Shan) revealed by 1976 KH-9 Hexagon and 2009 SPOT-5 stereo imagery

Tino Pieczonka [a,*], Tobias Bolch [a,b], Wei Junfeng [c], Liu Shiyin [c]

[a] Institute for Cartography, Technische Universität Dresden, 01069 Dresden, Germany
[b] Department of Geography, University of Zurich, 8057 Zürich, Switzerland
[c] State Key Laboratory of Cryosphere and Environment, Cold and Arid Regions Environmental and Engineering Research Institute, Chinese Academy of Sciences, Lanzhou 730000, China

ARTICLE INFO

Article history:
Received 31 May 2012
Received in revised form 16 November 2012
Accepted 17 November 2012
Available online xxxx

Keywords:
DTM
Change assessment
Geodetic glacier mass budget
Central Tien Shan
SPOT-5
KH-9 Hexagon

ABSTRACT

The meltwater released by the glaciers in the Aksu-Tarim Catchment, south of Tomur Peak (Central Tien Shan), feeds the Tarim River which is the main artery for the oases at the northern margin of the Taklamakan desert. The correct modeling of the contribution of the glaciers meltwater to the total runoff of the Tarim River is hampered by the lack of mass balance data. Multi-temporal digital terrain models (DTMs) allow the determination of volume changes for large samples of glacier. Here, we present the mass changes for 12 glaciers using 1976 KH-9 Hexagon, 2000 SRTM3 and 2009 SPOT-5 datasets. The results show that most of the glaciers have been losing mass since 1976. The largest glaciers, Koxkar and West Qongterang, lost -0.27 ± 0.15 m w.e.a^{-1} and -0.43 ± 0.15 m w.e.a^{-1} between 1976 and 2009, despite thick debris cover. However, some smaller glaciers show mass gain at their tongues indicating glacier surges. Using SRTM3 data the volume gain of Qinbingtan Glacier No. 74 could be dated to the time period 1999–2009. The overall mass budget of -0.33 ± 0.15 m w.e.a^{-1} (for 1976–2009) of the investigated glaciers is within the variability range of the global average. However, in the recent years (1999–2009) a slightly decelerated mass loss of -0.23 ± 0.19 m w.e.a^{-1} could be observed.

1. Introduction

The Tarim River in the northwestern part of China is nourished to a high degree by glacier meltwater (Kaser et al., 2010; Mao et al., 1998) and he is the main artery for the oases at the northern margin of the Taklamakan desert. Changes in glacier melt can therefore alter the runoff of the whole Tarim River. Several studies have reported an accelerated glacier retreat and mass loss in the Tien Shan Mountains (Kutuzov & Shahgedanova, 2009; Narama et al., 2010; Sorg et al., 2012; Wang et al., 2009; Xie et al., 2007). Runoff measurements for Aksu River indicate in general an increase of runoff (Fan et al., 2011). However, at Xehera station a deceleration of annual runoff in the last decade comparing to the decades before 2000 were measured (Yu et al., 2011). The contribution of glacial melt, however, is fuzzy and hard to quantify.

Therefore, changes in glacier coverage and mass in the Tien Shan Mountains and in Central Asia should be monitored continuously. While area and length changes can be derived relatively easy from remote sensing imagery (Bhambri & Bolch, 2009; Bolch et al., 2010; Paul et al., 2004; Zhou et al., 2009), only changes in glacier thickness can directly be related to glacier mass changes and the hydrology.

Multi-temporal digital terrain models (DTMs) were shown to be suitable to assess glacier mass changes (Aizen et al., 2006; Berthier et al., 2007; Bolch et al., 2011; Miller et al., 2009). However, missing reliable ground truth in remote mountainous areas hamper the generation of precise elevation datasets. Therefore, several studies related to glacier thickness change calculations rely on ancient topographic maps (Wang et al., 2009) or recent satellite datasets with appropriate sensor and orbit parameters. SPOT-5 stereoscopic imagery, in particular, was proved to be suited to monitor glacier elevation changes (Berthier & Toutin, 2008).

The declassification of Corona and KH-9 Hexagon reconnaissance satellite imagery in 1995 and 2002 offers a huge potential for DTM generation representing conditions in the past (Pieczonka et al., 2011; Surazakov & Aizen, 2010). In comparison to Corona imagery, KH-9 Hexagon offers the advantage of larger footprints without complex panoramic distortions while preserving a high spatial resolution of 6–10 m which is only slightly lower to that of Corona imagery. Working with multi-temporal DTMs necessitates a proper co-registration of all used datasets. Moreover, elevation biases have to be accounted for in order to avoid over- or underestimations of volume changes (Nuth & Kääb, 2011; Pieczonka et al., 2011).

Besides for the Ak-Shirak Range (Aizen et al., 2006) there exists no comprehensive investigation of glacier elevation changes in the Tien Shan (Sorg et al., 2012) including the region south of Tomur Feng (7439 m a.s.l., Kyrgyz name: Jengish Chokusu; Russian name: Pik

* Corresponding author at: Institute for Cartography, Helmholtzstraße 10, 01069 Dresden, Germany. Tel.: +49 35146333281; fax: +49 35146337028.
E-mail address: t.pieczonka@tu-dresden.de (T. Pieczonka).

0034-4257/$ – see front matter © 2012 Elsevier Inc. All rights reserved.
http://dx.doi.org/10.1016/j.rse.2012.11.020

Pobedy), which is one of the largest glacierized areas in the Central Tien Shan. Koxkar Glacier (also: Keqicar Glacier), solely, was investigated revealing a surface lowering of 0.5–1.5 m a^{-1} by analyzing 1981 and 2004 GPR measurements (Xie et al., 2007). These results shall be used to classify the results achieved by satellite stereoscopy.

The size of our study region is about 3000 km^2 located between 500 and 7439 m a.s.l.; ~800 km^2 of it are covered by glaciers. The most comprehensive and detailed investigated glacier in the study region with a width of 1–3 km, a length of more than 20 km and an area of 62 km^2 is Koxkar Glacier. Other large glaciers are Tomur Glacier and West Qongterang Glacier with heavily debris-covered glacier tongues and areas of 327 km^2 and 114 km^2 (Fig. 1, Table 1).

Therefore, one aim of this study is to calculate glacier thickness changes for a large sample of glacier south of Tomur Feng, Xingjiang Uighur Autonomous Region. Secondly, we want to show the suitability of KH-9 Hexagon stereoscopic images to derive glacier volume changes and to discuss the advantages and disadvantages of this data source.

2. Remote sensing datasets

Regarding the size of the study area and with respect to the desirable time span of more than 40 years which wanted to be covered by optical stereo satellite imagery we used KH-9 Hexagon and SPOT-5 stereo satellite images captured in 1976 and 2009 (Table 2). Glacier thickness investigations based on multi-temporal stereo satellite imagery necessitate, in dependency upon spatial resolution of input datasets, horizontal and vertical ground truth for GCP measurements. In remote mountain areas there is often a lack of precise ground truth datasets. Therefore, Landsat ETM+, SRTM3 and ICESat GLA 14 altimetry data were utilized as horizontal and vertical references.

2.1. KH-9 Hexagon

KH-9 Hexagon, the successor of the Corona missions, operated between 1971 and 1986 where 19 successful missions were accomplished (Center for the Study of National Reconnaissance, 2011). The sensor used a frame mapping camera similar to the Large Format Camera (LFC) with a 23×46 cm frame and a focal length of 30.5 cm (Surazakov & Aizen, 2010). The images of our study site were delivered by the USGS with a scan resolution of about 14 μm. Due to the long time of storage the image quality is impaired by age related mechanical damages like scratches. Additionally, we noticed vertical stripes which are well known artifacts in Corona imagery. Galiatsatos et al. (2008) traced them to the digital scanning where dust particles or calibration errors can affect the radiometric precision of a CCD scanner. Subsequently, radiometric discontinuities between successive matrix positions can occur.

2.2. SPOT-5

SPOT-5 was launched in May 2002 and is equipped with a HRS sensor and a HRG sensor; both offer stereoscopic capabilities. SPOT-5 HRS

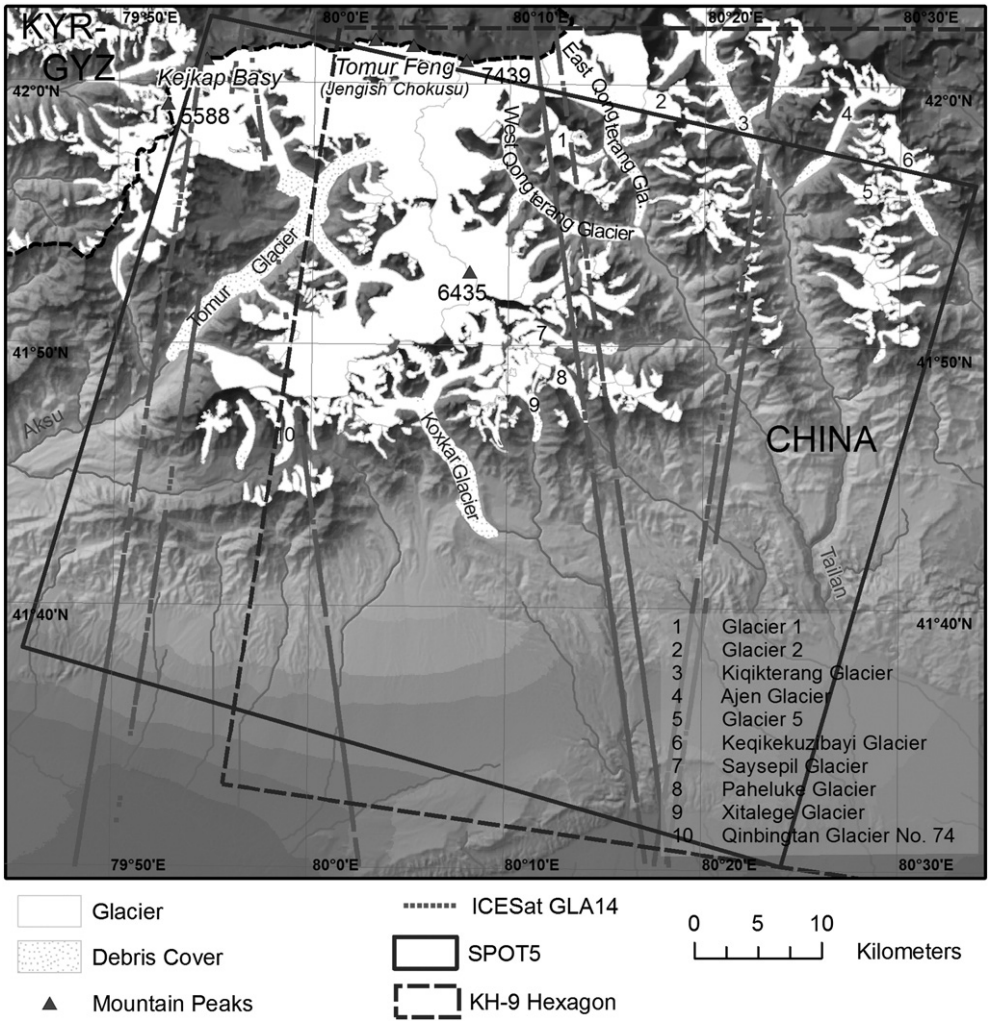

Fig. 1. Study area; names and location of the largest glaciers, coverage of the utilized satellite data. Background: SRTM3 GGIAR Vers. 4; glacier outlines based on 2009 SPOT-5 data.

Table 1
Overview and main morphologic characteristics of investigated glaciers.

Name/no.	WGI code	Lat/Lon	Aspect (ablation area)	Slope (ablation area)	Area	Length (ablation area)	Terminus altitude in 2009	Estimat. ELA based on CGI
			(degree)	(degree)	(km^2)	(km)	(m a.s.l).	(m a.s.l.)
Tomur	CN5Y673P0037	41.92/79.98	201.0 (SW)	9.8	327.4	28.8	2861.0	4350.0
West Qongterang	CN5Y674B0028	41.92/80.25	124.4 (SE)	10.3	114.8	16.6	3210.0	4300.0
Koxkar	CN5Y674A0005	41.77/80.11	150.7 (SE)	8.4	62.5	17.2	2999.0	4350.0
East Qongterang	CN5Y674B0028	41.96/80.28	165.7 (S)	12.1	52.3	12.8	3201.0	4300.0
Keqikekuzibayi	CN5Y674E0015	41.92/80.57	140.8 (SE)	13.0	13.1	6.3	3438.0	4180.0
Saysepil	CN5Y674B0016	41.83/80.22	95.2 (E)	11.8	11.7	7.0	3357.0	4240.0
Glacier 2	CN5Y674B0028	41.99/80.30	242.9 (SW)	9.3	7.5	2.8	3861.0	n.a.
Qinbingtan Glacier No. 74	CN5Y673P0077	41.77/79.96	185.0 (S)	7.1	6.2	3.3	3930.0	4400.0
Glacier 1	CN5Y674B0028	41.97/80.25	92.3 (E)	11.5	5.3	3.2	3803.0	n.a.
Glacier 5	CN5Y674C0022	41.95/80.50	314.3 (NW)	16.9	3.4	2.3	3867.0	4270.0
Paheluke	CN5Y674A0023	41.80/80.24	119.5 (SE)	12.6	4.7	4.8	3537.0	4260.0
Xitalege	CN5Y67A0014	41.78/80.20	150.7 (SE)	14.3	9.4	5.3	3446.0	4350.0
Average				15.3	55.5	13.3	3459.2	4293.3

ELA—Equilibrium Line Altitude, CGI—Chinese Glacier Inventory (Shi, 2008).

acquires stereoscopic images in an along-track mode. The sensor consists of two cameras – one pointing 20° forwards and one points 20° backwards – offering a base-to-height-ratio of about 0.8 (Korona et al., 2009). For our study we used two across-track stereoscopic images captured by the HRG sensor system on the first and second November 2009 in panchromatic mode (THR) under similar weather conditions. The images were captured with an incidence angle of −9.6° and 20.3° offering a base-to-height-ratio of about 0.6. Visual inspection of the images indicates two distinct zones—high mountains in the upper and lowlands in the lower part of the scene. While snow coverage is dominant in the high mountain area, the lowlands offer good contrast. A SPOT-5 scene can be located on the ground with an accuracy of ±25 m on the 66% confidence level because the orbit of the satellite is well known by INS systems (Berthier et al., 2007).

2.3. Landsat ETM + (Level 1T)

The Landsat ETM + (Level 1T) acquired on 20 July 2003 in the SLC (Scan Line Corrector) off mode was used as general horizontal reference. Because a main part of the study area is located within the center of the scene the failure of the scan line corrector in 2003 has not much impact. For Level 1G the accuracy is specified with a RMSE of <50 m (Tucker et al., 2004). In contrast to Level 1G Level 1T utilizes Ground Control Points (GCPs) coming from the GLS2005 (Global Land Survey) dataset to attain absolute geodetic accuracy (http://landsat.usgs.gov/products_productinformation.php). A visual comparison of mountain ridges derived from SRTM3 and GLS2005 revealed no horizontal offset; thus, we assume a horizontal accuracy of Landsat ETM + (Level 1T) similar to that of SRTM3.

2.4. SRTM3

DTM generation needs a height reference of superior accuracy. As no high resolution DTM was available for this region we utilized the original SRTM data (http://dds.cr.usgs.gov/srtm/version2_1/SRTM3/) and the processed SRTM3 data of the Consultative Group for International Agricultural Research (CGIAR), version 4 (http://srtm.csi.cgiar.org/) whose data gaps were filled by means of ancillary elevation data (Reuter et al., 2007). The original SRTM3 dataset acquired in early February 2000, which elevations are roughly referring to the 1999 glacier surface, was used to evaluate our DTMs and to derive glacier elevation changes whereas the processed SRTM3 CGIAR DTM was used to generate orthophotos of the SPOT-5 images. The accuracy of SRTM3 DTMs is specified with 20 m in xy-directions and 16 m in z-direction within the 90% confidence coefficient (Falorni et al., 2005). Flat areas, in particular, can show a RMSEz below 10 m whereas steep slopes might have even higher elevation errors (Rodriguez et al., 2006).

2.5. ICESat GLAS

The Ice, Cloud and Land Elevation Satellite (ICESat) was launched in 2003 and is specially targeted for investigations in Polar Regions. The onboard Geoscience Laser Altimeter System (GLAS) acquires elevation measurements in an approximately 65–70 m footprint with 175 m center-to-center separation. The horizontal and vertical accuracy are determined with 10.6 ± 4.5 m and 34 cm (Magruder et al., 2007). As ICESat GLAS elevations shall be used as vertical reference for stable ground control points the GLA 14 product was selected as suggested by Nuth and Kääb (2011) and Kääb (2008). The GLA 14 elevations correspond to the centroid of the received waveform (Harding & Carabajal, 2005). The data were transformed from the TOPEX/Poseidon ellipsoid to the WGS 84 ellipsoid. To reduce slope effects footprints on steep areas (slope angle > 15°) were excluded. Assuming a slope induced elevation error of about 10–15 cm per 2° slope (Beaulieu & Clavet, 2009) a threshold of 15° was chosen in order to ensure a vertical accuracy ≤1 m. Incorrect elevation values, e.g. caused by clouds, were detected and eliminated by comparing with the elevations of the original SRTM3 dataset and adjacent ICESat tracks from different dates. As threshold we used the vertical standard error of SRTM3 of 10 m.

Table 2
Utilized input and reference datasets.

Sensor	Date	Coverage	Operation	Spatial res.	Rad. res.	Stereo
Input						
KH-9 Hexagon	12/01/1976	~250 × 125 km^2	1971–1986	7.6 m	8 bit	Yes
SPOT-5	01/11/2009	60 × 60 km^2	Since 2002	2.5 m	8 bit	Yes
Reference						
Landsat ETM +	20/07/2003	183 × 170 km^2	Since 1999	14.25 m	8 bit	
SRTM (STS-99)	11/02/2000	1° × 1° (tile size)	Feb. 2000	90 m		
ICESat (GLA14)	2003–2009		Since 2003	65 m		

3. Data pre-processing, DTM generation and glacier mapping

Data preprocessing comprises radiometric as well as geometric corrections. Here, most of the work is devoted to the KH-9 Hexagon images. These images are characterized by 1058 reseau crosses whose position was automatically determined using the Python Imaging Library (PIL). To discriminate the reseau crosses from the local neighborhood their contrast was enhanced applying the Wallis filter and histogram equalization. Thus, the reseau crosses could be determined with subpixel accuracy and used to constitute the image geometry at the time of image exposure. Assuming a grid spacing of 10 cm between adjacent reseau crosses the nominal positions were determined and a second order polynomial bilinear interpolation was performed to correct the image geometry (cf. Surazakov & Aizen, 2010). Comparing nominal and measured positions a mean image distortion of about 0.93 pixel (12.9 μm) had to be corrected. In the last step the reseau crosses were interpolated through a bicubic spline surface considering neighboring pixel values.

Different intensities of snow and cast shadows are problematic in terms of image matching. Therefore, we applied a radiometric enhancement by implementing the locally adaptive Wallis Filter which is designed for grayscale images with distinct areas of bright and dark tones to adjust the brightness values in local areas (Baltsavias et al., 2007). With respect to the amount of snow and shadow we chose a window size of 50×50 pixels, a local mean of 121 and a threshold of 65 for the standard deviation.

A rule of thumb used for photogrammetric DTMs can give a first guess regarding the expected accuracy of DTMs. For moderate mountainous terrain a vertical RMSE of about 1–3 times the image pixel size can be achieved. Such areas can be found in the foothills of the Tien Shan Mountains. A RMSE of 5–7 times the image pixel size can be expected for rough topography (Kääb, 2010). Thus, considering the spatial resolution of the KH-9 Hexagon dataset the final DTM will have a RMSE between 15 and 40 m.

The main point of DTM generation using optical stereo imagery is the restitution of the camera situation at the time of image exposure. Therefore, GCPs (Ground Control Points) have to be measured based on horizontal and vertical reference datasets. As horizontal reference Landsat ETM + Level 1T was used. We orthorectified a SPOT-5 scene from 2009 with a spatial resolution of 2.5 m using Landsat ETM + and SRTM3 CGIAR with a RMS error of 4.2 pixel (≈10.5 m) to take advantage of the higher spatial resolution in comparison to 14.25 m of the Landsat ETM + image.

For flat areas with slope angles less than 15° we used ICESat GLAS 14 elevation values instead of SRTM3 whose pixel location was identified using the rectified SPOT-5 image. To ensure an even distribution of the GCPs SRTM3 elevations were used for areas outside ICESat tracks.

In total, 38 GCPs were measured on distinct topographic terrain features, like river junctions and mountain ridges. We used the same set of GCPs for the KH-9 and SPOT-5 dataset with regard to a good relative accuracy.

The processing of KH-9 Hexagon was done with Leica Photogrammetry Suite 9.2. (LPS). In addition, SPOT-5 was also processed using PCI Geomatica OrthoEngine 2012 (PCI) to test different sensor models. The residuals are listed in Table 3.

The sampling distance of the final DTMs was chosen as 25 m for both the SPOT-5 and the KH-9 Hexagon DTM. As reference coordinate system we utilized UTM zone 44 with WGS 84 as reference ellipsoid.

The post-processing of the final DTMs encompassed the data gap handling. We transformed our DTMs to a binary image and applied mathematical morphology to make frayed data gaps more compact and to remove elevation values close to data gaps. Small data gaps (<0.04 km^2), disappearing after the close operator, were afterwards interpolated bilinearly using the original elevation values.

A high relative accuracy has to be established by removing horizontal displacements and vertical elevation differences for non-glacierized areas to make the DTMs suitable for glacier thickness change calculations. The corresponding glacier outlines, inevitable in order to distinguish between stable and non-stable terrain for DTM accuracy analysis, were downloaded from the GLIMS database (Li, 2003) and manually refined using a SPOT-5 stereo anaglyph enabling a clear discrimination between different glacier subbasins. In a last step rock glaciers and ice-cored moraines were delineated and excluded from the analysis. Some rock glaciers could not be clearly distinguished from debris-covered glaciers in this region where permafrost is likely in the elevations were glaciers occur (Gruber, 2012). Typical signs for rock glaciers like ridges and furrows and a fresh, steep front provided evidences for rock glaciers.

Table 3
Residuals after stereo model adjustment.

[m]	KH-9 Hexagon[a]	SPOT-5[a]	SPOT-5[b]
No. GCP	38	38	38
RMSEx	13.43	7.99	4.75
RMSEy	13.39	5.22	3.39

[a] LPS.
[b] PCI Geomatica.

Comparing with SRTM3 elevation values, the penetration depth of the radar beam into ice and snow needs to be considered. The penetration depth is strongly influenced by a variety of parameters such as dielectric properties of snow, snow temperature, density, age and snow structure (König et al., 2001). A snow mask was generated applying the Normalized Difference Snow Index (NDSI) with a threshold of 0.4 to a Landsat ETM + (Level 1T) scene captured on 18 February 2000 in order to get the approximate snow extent at the time of the SRTM mission. Under dry snow conditions the C-band (6 GHz) may represent the ground surface characteristics underlying the snow pack whereas the X-band (10 GHz) does not (Gardelle et al., 2012a). To filter the penetration depth from the C-band the mean value of the differences between X-band and C-band, limited to the snow covered accumulation areas with a slope angle <10° (Gorokhovich & Voustianiouk, 2006), was calculated.

4. DTM accuracy and DTM enhancement

The quality of a DTM depends on several parameters like image contrast, the interpolation technique, quality of Ground Control Points and the general topography of the area under investigation. The significance of an accuracy evaluation mainly depends on the availability of reference datasets of superior quality and accuracy.

DTM accuracies can be evaluated in terms of their absolute and relative accuracy. To ensure exact absolute accuracy evaluations field based measurements are indispensable. In this study we analyzed the relative accuracy of our multi-temporal DTMs against ICESat GLAS footprint elevation values as a reference dataset with submeter accuracy. In a second step, we evaluated the relative accuracy of our DTMs relative to each other. Comparing to different sets of elevation data necessitates the adaptation of the spatial resolutions to that of the coarsest DTM and the exclusion of areas which are not supposed to be stable over multi-decade time periods. This encloses e.g. glaciers, rock glaciers and ice-cored moraines.

In total 1831 ICESat GLA14 footprints, measured between 2003 and 2009, were available. They were located on non-glacierized terrain below a slope angle of 15°. This is higher than the slope angle of 3° suggested by Surazakov and Aizen (2010), but still suitable by an expected DTM elevation error of 15–40 m.

The best relative accuracy, when comparing with ICESat GLA 14 footprint elevation values, was achieved for the SPOT-5 PCI DTM with a RMSEz of 11.03 m (Fig. 2; Table 4). Therefore, this DTM was successively be used as the reference (master) DTM for the relative

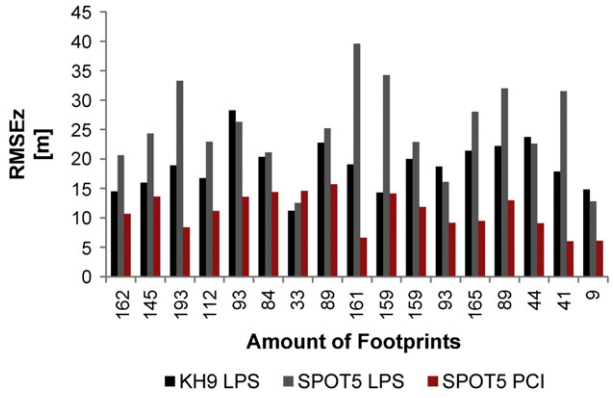

Fig. 2. RMSEz of elevation differences between ICESat GLA14 footprints and SPOT-5/KH-9 elevation values (ICESat footprints are limited to slope angles <15°).

Table 4
RMSEz for non-glaciated areas in comparison to ICESat GLA 14 elevation values.

KH-9 LPS	SPOT-5 LPS	SPOT-5 PCI
18.87 m	25.07 m	11.03 m

Date of GLA14 footprints: October 2003, February/June/November 2004, February/May/October 2005, February/May/October 2006, April/November 2007, February/October/December 2008, March/October 2009.

accuracy analysis and adjustment. KH-9 Hexagon and SRTM3 are used as slave DTMs.

Based on a difference image between master and slave DTMs the overall relative accuracy was determined. In a first step the 5% and 95% quantiles were set as bounds to eliminate the most extreme outliers. The remaining pixels were then utilized to calculate the interquartile range (IQR). The final set of pixels used to assess the horizontal and vertical fitting of both DTMs was composed of all pixels lying between the two-tailed 1.5 times IQR.

Two DTMs that are not perfectly aligned tends to falsify glacier thickness calculations. In accordance to Nuth and Kääb (2011) we checked our DTMs against horizontal displacements and elevation dependent errors and used their analytical approach to co-register our DTMs properly. Nuth and Kääb (2011) pointed out a strong relation between horizontal shifts and the corresponding slope and aspect values at a certain pixel position. Aspect values must be adjusted by taken potential nonconformities in the terrain into consideration. Therefore, we excluded all pixels with a slope angle less than 5° as these aspect values might be falsified by inherent elevation errors. The linear equation system is solved by a least-square optimization based on Fourier analysis. The final magnitude and direction of the shift vector are calculated from the coefficients of the Fourier series. We stopped the iteration when the length of the shift vector had fallen below 1 m. Remaining elevation differences were minimized based on spatial trend corrections (cf. Pieczonka et al., 2011). In this case we used a second order trend surface, representing the global trend towards the calculated height differences over non-glacierized areas, to adjust the slave DTM.

DTMs are also characterized by a certain degree of autocorrelation; therefore, we chose an autocorrelaction distance of 400 m (Bolch et al., 2011; Nuth & Kääb, 2011).

To prove a potential horizontal displacement between both DTMs we depict the difference values, which are outlier-cleaned and standardized on the basis of the slope angle, in dependence upon aspect (Fig. 3). There is a substantial sinusoidal relationship indicating a north–south oriented horizontal displacement between SPOT-5 and KH-9 and SPOT-5 and SRTM3. The final shift vectors are listed in Table 6. For cross-checking we also determined the shift vector between KH-9 and SRTM3. The shift vector from KH-9 and SPOT5 is −13.4 m in x-direction and 9.0 m in y-direction. However, the shift vector from KH-9 to SPOT5 via SRTM3 is slightly different with −30.0 m in x-direction and 1.7 m in y-direction which is caused by the lower morphological and spatial resolution of SRTM3. Remaining elevation dependent biases were afterwards removed by a second order trend surface. As a result the RMSEz decreased by 23.4% for the KH-9 DTM and 62.4% for SRTM3 in relation to the SPOT-5 Master DTM (Table 5).

A comparison between SRTM C-band and X-band revealed an average penetration depth of the C-band radar beam into snow of about only 0.3 m. This is lower than the 3 m penetration depth reported by Gardelle et al. (2012a) for the Karakoram indicating little snow cover at the time of acquisition. The discrepancies of the penetration depth of the C-band signal in comparison to the Karakoram region might be explained by different local climatic conditions and different precipitation regimes (Bolch et al., 2012; Sorg et al., 2012). Otherwise, a thin snowpack in February 2012 will also implicate a slight penetration of the radar beam.

In consideration of the vertical accuracy of SRTM3 elevation datasets the measured penetration depth is not significant.

To describe the accuracy of the relative fitting of two DTMs we calculated the root mean square error (RSME), mean, median, and standard deviation. The RMSE is not the best description of the statistical distribution of the relative elevation error, if the mean error is unequal to zero. Therefore, the mean error and the mean standard deviation should be reported (Fisher & Tate, 2006). As a robust estimator for the standard deviation, resistant to scattered outliers, we used the Normalized Median Absolute Deviation (NMAD) (Höhle & Höhle, 2009).

The change rates for a glacier are usually described by the average value over the whole glacier. Nuth and Kääb (2011) proposed the standard error, indicating the fuzziness of the mean value, to account for this fact. The standard error considers the amount of un-correlated

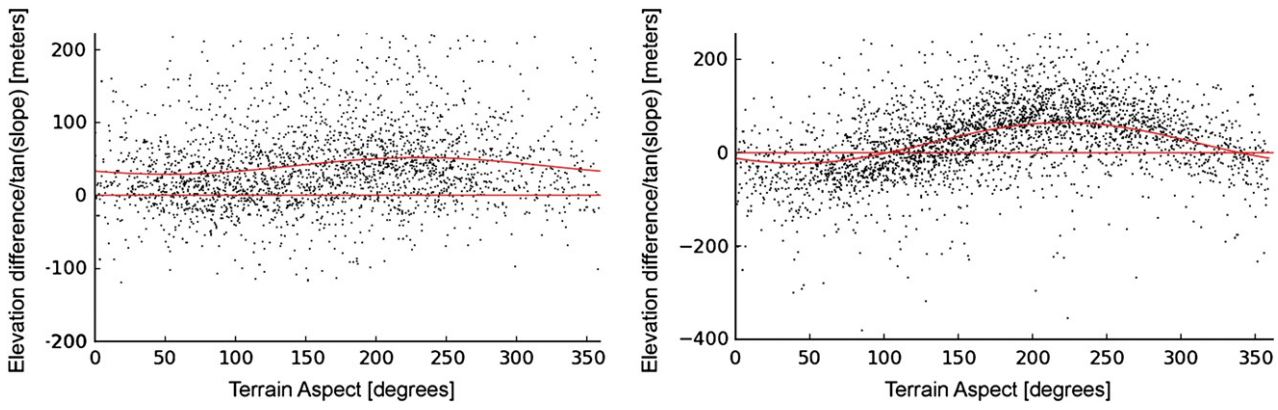

Fig. 3. Left: Scatterplot of slope standardized elevation differences of SPOT-5–KH-9 vs. aspect, Right: Scatterplot of slope standardized elevation differences of SPOT-5–SRTM3 vs. aspect.

Table 5
Statistics for non-glaciated areas.

	RMSEz (m)	Mean (m)	STD (m)	MED (m)	MIN (m)	MAX (m)
SPOT-5–KH-9						
Original	17.1	10.5	13.5	10.5	−20.5	41.0
Adjusted	13.1	−0.8	13.1	−0.9	−31.3	29.4
SPOT-5–SRTM3						
Original	22.3	7.5	21.1	6.8	−40.6	57.0
Adjusted	8.4	−0.8	8.4	−1.1	−19.9	19.3

Table 6
Shift vectors in x, y and z direction.

KH-9 −> SPOT-5			SPOT-5 <− SRTM3			KH-9 −> SRTM3		
X (m)	Y (m)	Z (m)	X (m)	Y (m)	Z (m)	X (m)	Y (m)	Z (m)
−13.4	9.0	11.6	−72.9	−70.2	4.0	40.2	71.9	5.9

pixels; thus, the error will decrease with increasing sample size equitable to a large study area. Hence, the uncertainty might be underestimated.

In accordance to Höhle and Höhle (2009) we decided to calculate the bootstrap based 95% confidence interval to assess the uncertainty of the sample mean values. The sample size and the number of repetitions were defined with 100 and 999. Additionally, the standard error is determined as the variance of the sample mean values. In order to take non-normality into account the 68.3% quantile is calculated (Table 7). The 68.3% quantile indicates the limit in which 68.3% of the absolute elevation differences are situated. In case of normality the 68.3% quantile encompasses all values within the single standard deviation. Therefore, we checked the sample values against normality using Q-Q plots and report the standard deviation in case of normality and the 68.3% quantile in case of non-normality in order to describe the quality of glacier volume measurements.

For the calculation of glacier thickness changes, we selected 12 glaciers distributed over the whole study area with different glacier tongue expositions. The glaciers were selected regarding size, DTM coverage and the amount of pixels in both, the ablation and accumulation areas.

To exclude false values from matching failures only difference values between the 1.5 times IQR are considered in the calculation of thickness changes. This comprises all values between −79.8 m and 52.0 m for the SPOT-5–KH-9 difference image and −70.4 m and 77.8 m for the SPOT-5–SRTM3 differences. As the height error increases with the slope angle only pixels on slopes lower than 30° were considered (Pieczonka et al., 2011). The Q-Q plots indicate non-normality and the NMAD value and the 68.3% quantile differ strongly. Therefore, the 68.3% quantile is used as quality criterion for glacier volume measurements.

To separate between accumulation and ablation areas, we assumed an equilibrium line altitude (ELA) of 4300 m a.s.l. This value is based on the Glacier Inventory of China and was measured indirectly using topographic maps (Shi, 2008). We are aware that the ELA is not the same for all glaciers due to different morphologies and varying elevation ranges covered by them. To get precise ELA values continuous mass-balance measurements are necessary for each glacier (Iwata, 2009). We considered two different assumptions for the accumulation areas as the topography in the accumulation region supports elevation inaccuracies in the DTMs. In our first assumption we assumed no elevation changes for missing pixel values in the accumulation area, i.e. the downwasting rate results from the quotient of the sum of the existing pixel values and the total accumulation area of a specific glacier (S1). This assumption is supported by the fact that the elevation change in the accumulation area is low over the period of several decades (Schwitter & Raymond, 1993). In the second assumption the mode value of the elevation differences in the accumulation area of a glacier should be applied to the whole accumulation area of the same glacier (S2). The representativeness of the mode values for the accumulation areas are corroborated by Paul and Haeberli (2008). Using the example of the Swiss Alps they refuted an underestimation of SRTM3 elevations in accumulation regions investigating climatic conditions and glacier surface characteristics. However, the representativeness of the mode value is limited by the rate of missing grid values in accumulation areas and the available sample size.

Mass budgets are calculated based on commonly used parameters for glacier ice density (900 kg/m^3) and water density (999.972 kg/m^3) (Bolch et al., 2011; Rivera et al., 2005). Assuming that the sample glaciers are representative for the whole region south of Tomur Peak the overall glacier area mass budget for the study area was calculated as the weighted average.

5. Glacier changes

Most of the glaciers show a significant surface lowering in the ablation areas of -18.7 ± 5.6 m for the 1976–2009 period (Fig. 4). Between 1999 and 2009 the downwasting continued with an additional lowering of -6.7 ± 2.1 m (-0.67 ± 0.21 m a^{-1}) which was lower than between 1976 and 1999 with about -22.6 ± 5.8 m (0.98 ± 0.25 m a^{-1}). The overall mass budgets of the investigated glaciers for the 1976–1999, 1976–2009 and 1999–2009 time periods were -0.42 ± 0.23 m w.e.a^{-1}, -0.35 ± 0.15 m w.e.a^{-1} and -0.23 ± 0.19 m w.e.a^{-1} (Tables 8–10). The overall mass loss of all the glaciers south of Tomur Peak (total area 846.1 km^2) for the periods were -0.48 ± 0.23 m w.e.a^{-1}, -0.33 ± 0.15 m w.e.a^{-1} and -0.23 ± 0.19 m w.e.a^{-1} assuming that the investigated glaciers are representative for the region. The average thickness loss of Koxkar Glacier over the whole glacier area for the time periods 1976–1999, 1976–2009 and 1999–2009 were determined with -8.9 ± 5.8 m (-0.39 ± 0.25 m a^{-1}), -9.7 ± 5.6 m (-0.29 ± 0.17 m a^{-1}) and -0.9 ± 2.1 m (-0.09 ± 0.21 m a^{-1}).

In contrast to Koxkar Glacier, Qinbingtan Glacier No. 74 showed a comparatively large volume gain in the recent years with an estimated positive mass budget between 1999 and 2009 of 0.24 ± 0.19 m w.e.a^{-1}. The volume change shows typical characteristics of a glacier surge—a significant thickening at the glacier tongue and a clear lowering above. Hence, the assumption with no elevation changes in the accumulation area is not valid for this glacier. A visual inspection of the elevation differences of Qinbingtan Glacier No. 74 confirms this different behaviors. Hence, we closed the gap in the accumulation area for the 1999–2009 period linearly (Fig. 8) and used the central value of −10 m as the estimated average elevation change in the whole accumulation area.

The overall mass budget of Qinbingtan Glacier No. 74 is, however, negative with -0.80 ± 0.15 m w.e.a^{-1} between 1976 and 2009.

Table 7
Glacier statistics for the investigated time period.

Period	DTM coverage study area (km^2)	DTM coverage glac. (km^2)	Mean elev. diff. no. glac. (m)	STDV no. glac. (m)	Mean elev. diff. glac. (m)	STDV glac. (m)	Q68.3 no. glac. (m)	NMAD no. glac. (m)
1976–1999	2332.3	459.7	0.5	11.0	−23.8	21.4	5.8	10.8
1976–2009	2310.5	450.9	−0.8	13.1	−13.2	27.9	5.6	13.4
1999–2009	2942.8	569.6	−0.8	8.4	0.9	23.0	2.1	7.3

Table 8
Glacier volume losses and mass budgets for the time period 1976–2009 (an ice density of 900 kg/m^3 is used for mass balance calculations).

Glacier	Glacier size (km^2)	Glacier area covered by DTM (km^2)	Rate of missing grid values accum. area (%)	Average elev. diff. ablation area (m)	Specific mass budget (m w.e.a^{-1})
Tomur	327.4	82.2		−35.1 ± 5.6	n.c.
West Qongterang	115.9	63.1	59.2	−26.5 ± 5.6	−0.43 ± 0.15[a]
Koxkar	63.1	39.3	63.0	−18.0 ± 5.6	−0.27 ± 0.15
East Qongterang	52.9	10.9		−32.8 ± 5.6	
Keqikekuzibayi	13.1	4.8		−20.9 ± 5.6	n.c.
Saysepil	11.7	8.5	45.7	−6.5 ± 5.6	−0.08 ± 0.15
Glacier 2	7.5	2.1	93.9	−28.8 ± 5.6	−0.27 ± 0.15
Qinbingtan Glacier No. 74	6.6	3.3	87.5	−34.0 ± 5.6	−0.80 ± 0.15
Glacier 1	5.3	2.6	71.5	−21.2 ± 5.6	−0.41 ± 0.15
Glacier 5	3.4	2.5	35.6	−20.4 ± 5.6	−0.30 ± 0.15
Paheluke	4.7	2.5	26.9	5.4 ± 5.6	0.33 ± 0.15
Xitalege	9.4	6.0	48.3	8.0 ± 5.6	0.21 ± 0.15
Total glacier area	846.1	340.8		−18.7 ± 5.6	−0.35 ± 0.15

[a] Mode value used for accumulation area n.c.: not calcualted as only a small portion of the ablation area is covered.

Table 9
Glacier volume losses and mass budgets for the time period 1976–1999 (an ice density of 900 kg/m^3 is used for mass balance calculations).

Glacier	Glacier size (km^2)	Glacier area covered by DTM (km^2)	Rate of missing grid values accum. area (%)	Average elev. diff. ablation area (m)	Specific mass budget (m w.e.a^{-1})
Tomur	327.4	89.1		−34.5 ± 5.8	n.c.
West Qongterang	115.9	59.1	76.5	−21.7 ± 5.8	−0.62 ± 0.23
Koxkar	63.1	42.8	62.7	−12.7 ± 5.8	−0.35 ± 0.23
East Qongterang	52.9	19.4		−25.5 ± 5.8	n.c.
Keqikekuzibayi	13.1	5.7		−32.9 ± 5.8	
Saysepil	11.7	7.5	81.0	−5.6 ± 5.8	−0.16 ± 0.23
Glacier 2	7.5	3.5	73.1	−24.4 ± 5.8	−0.49 ± 0.23
Qinbingtan Glacier No. 74	6.6	3.5	82.9	−52.4 ± 5.8	−1.53 ± 0.23
Glacier 1	5.3	2.0	95.7	−25.0 ± 5.8	−0.82 ± 0.23
Glacier 5	3.4	2.7	57.0	−33.4 ± 5.8	−1.02 ± 0.23
Paheluke	4.7	3.7	54.0	0.0 ± 5.8	0.00 ± 0.23
Xitalege	9.4	6.9	46.7	3.3 ± 5.8	0.05 ± 0.23
Total glacier area	846.1	374.6		−22.6 ± 5.8	−0.42 ± 0.23

We identified a volume gain in the central part of West Qongterang Glacier tongue (Fig. 6C). Taking into account the spatial distribution of the elevation differences of West Qongterang Glacier we assumed the mode as the best guess for the accumulation area. The mass budgets between 1976–1999, 1976–2009 and 1999–2009 are negative with −0.62 ± 0.23 m w.e.a^{-1}, −0.43 ± 0.15 m w.e.a^{-1} and −0.47 ± 0.19 m w.e.a^{-1}. Before 1999 glacier thinning was mainly concentrated to the lower part of the glacier tongue (Fig. 6A), whereas in the recent years a strong mass loss was encountered in the upper part of the ablation area. In the same time the surface lowering decreased from −26.5 ± 5.6 m between 1976 and 2009 to −12.8 ± 2.1 m between 1999 and 2009 (Table 8; Table 9; Table 10).

6. Discussion

Existing studies of glacier area changes in Tarim River basin reveal an overall shrinkage. The glaciers in the Central Chinese Tien Shan shrank by 11.5% during the past 50 years (Wang et al., 2011b) while the glacier area of the Tarim River Basin in China decreased by 4.6% in the recent 40 years (Liu et al., 2006). A slight area loss of ~2.9% between 1970 and 1999 was observed for the glaciers in the Karamila–Keriya River watershed in the southern Tarim Basin (Xu et al., 2006).

Xie et al. (2006) found a complex pattern of stagnant periods, periods of advance and retreat for Koxkar Glacier which could also be observed for other glaciers in the study area (Table 11). Stagnant

Table 10
Glacier volume losses and mass balances for the time period 1999–2009 (an ice density of 900 kg/m^3 is used for mass balance calculations).

Glacier	Glacier size (km^2)	Glacier area covered by DTM (km^2)	Rate of missing grid values accum. area (%)	Average elev. diff. ablation area (m)	Specific mass budget (m w.e.a^{-1})
Tomur	327.4	152.5	68.4	−15.2 ± 2.1	−0.69 ± 0.19
West Qongterang	114.8	45.7	76.9	−12.8 ± 2.1	−0.47 ± 0.19[a]
Koxkar	62.5	35.2	71.1	−3.5 ± 2.1	−0.08 ± 0.19
East Qongterang	52.3	9.7		−12.3 ± 2.1	n.c.
Keqikekuzibayi	13.1	4.9		1.9 ± 2.1	n.c.
Saysepil	11.7	6.7	73.0	−1.2 ± 2.1	−0.02 ± 0.19
Glacier 2	7.5	2.0	94.5	−10.4 ± 2.1	−0.42 ± 0.19
Qinbingtan Glacier No. 74	6.2	4.2	52.5	16.5 ± 2.1	0.24 ± 0.19
Glacier 1	5.3	1.8	93.5	−6.6 ± 2.1	−0.22 ± 0.19
Glacier 5	3.4	2.5	43.1	−1.7 ± 2.1	−0.04 ± 0.19
Paheluke	4.7	2.6	31.1	1.5 ± 2.1	0.51 ± 0.19
Xitalege	9.4	5.3	56.0	5.4 ± 2.1	0.48 ± 0.19
Total glacier area	839.9	386.2		−6.7 ± 2.1	−0.23 ± 0.19

[a] Mode value used for accumulation area.

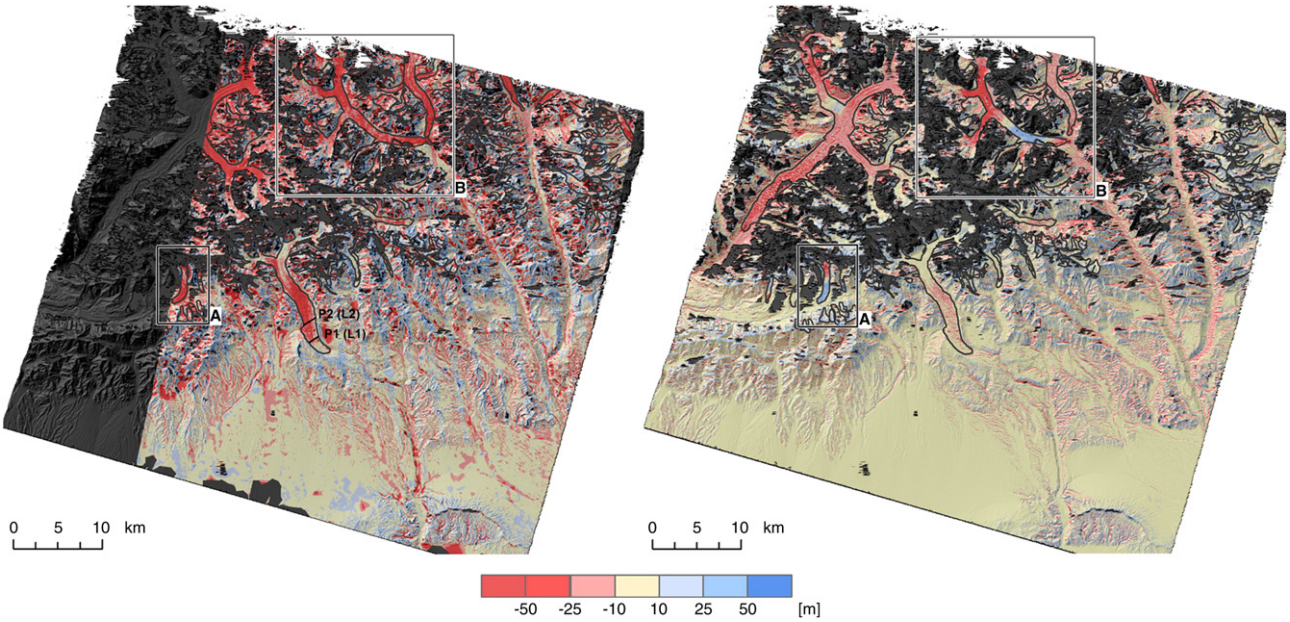

Fig. 4. Left: Adjusted difference image between SPOT-5 and KH-9 (vertical stripes caused by digital scanning of KH-9 frames are clearly visible), Right: Adjusted difference image between SPOT-5 and SRTM3. Detailed maps of A and B are shown on Figs. 5 and 6.

periods were identified between 1976 and 1981 followed by years of retreat until 1984. The consecutive years until 1990 were characterized by years of stability. Since 1990 the glacier tongue retreated with an accelerated speed. Koxkar Glacier has also been subject to detailed investigations regarding glacier melting rates and glacier runoff (Xie et al., 2006, 2007). Xie et al. (2007) conducted and analyzed glacier thickness measurements on Koxkar Glacier by Ground Penetrating Radar (GPR). For two transects, measured in 1981 and 2004, at the lower part of the glacier tongue (at an altitude of 3170 m a.s.l. and 3300 m a.s.l.) they determined a surface lowering of 11 m and 17 m with a rate of decrease of about 0.5 m a^{-1}. For the upper part of the glacier tongue they estimated the speed of thinning to be about 1 m a^{-1}. To validate our measurements we measured two profiles P1 and P2 whose positions coincide with that of the GPR measurements (Fig. 7). The averaged thinning is 16.6 m for P1 and 24.5 m for P2 showing an advanced glacier lowering.

The mean annual surface lowering for the ablation area of Koxkar Glacier of about 0.54 ± 0.16 m w.e.a^{-1} in the time period 1976–2009 is similar to the estimated surface elevation change determined by Xie et al. (2007) of about −0.5–1.0 m between 1981 and 2005. In the recent years field based mass budget measurements were realized on Koxkar Glacier. The mean mass budgets of the Koxkar Glacier were measured to be −494 and −384 mm w.e. in the mass budget year of 2003/2004 and 2004/2005 (Zhang et al., 2006). Thus, the average of −0.44 m w.e.a^{-1} is higher than the mass budget of -0.08 ± 0.19 m w.e.a^{-1} determined by DTM differencing (Table 10). The decelerated lowering of Koxkar Glacier might be explained by an increase of precipitation in the recent decades as reported by Shi et al. (2007). However, both results are not directly comparable as the investigations by Zhang et al. (2006) concentrate the measurements on the ablation area only and hence, further investigations are needed.

Table 11
Glacier length changes of selected glaciers (Shi et al., 2010).

Glacier	Period	Length change. (m a^{-1})
East Qongterang	1942–1976	−5
West Qongterang	1942–1976	−18
Kiqiterang	1942–1976	0
Saysepil	1942–1976	+62
Aylonsu	1946–1976	+53

Koxkar, West Qongterang and Tomur Glacier show significant volume losses with strong negative mass budgets since 1976 despite thick debris-cover (Table 8). These results are in line with other studies conducted in the Himalaya (Berthier et al., 2007; Bolch et al., 2012, 2011; Kääb et al., 2012) and Karakoram (Gardelle et al., 2012b).

Qinbingtan Glacier No. 74 (Fig. 5B) shows distinctive areas of volume gain and volume loss separated by a sharp border and a positive surface elevation change from 1999 to 2009 (Table 10). Hence, we checked the changes of this glacier from suitable Landsat ETM + images. Two available scenes from 2002 and 2010 show a glacier advance of ~90 m and a glacier area increase by 6.4% (Fig. 5D). This result is in agreement with the volume gain of this glacier between 1999 and 2009.

Distinct areas of volume gain and mass loss can also be recognized at West Qongterang Glacier. While a mass loss occurred in the upper part, a significant volume gain was measured in the central part of the glacier tongue (Fig. 6).

Together, all indicators add up to the assumption that Qinbingtan Glacier No. 74 and West Qongterang Glacier are surging glaciers. Additionally, the glacier advance of Qinbingtan Glacier No. 74 is out of phase comparing to the adjacent Qinbingtan Glacier No. 72 (Wang et al., 2011a) which is another evidence for a surge-type glacier (Copland et al., 2011). Existing investigations of glacier length changes in the study region show a complex behavior also before 1976 with advancing as well as retreating glaciers (Shi et al., 2010; Table 10). The surges might be caused by dynamic instability of the glacier system itself as it was observed for other glaciers in the Tien Shan Mountains (Dolgoushin & Osipova, 1975) and is also typical for glaciers in the Pamir (Kotlyakov et al., 2008) and the Karakoram (Bolch et al., 2012; Copland et al., 2011; Hewitt, 2007; Quincey et al., 2011).

The use of the mode value as indicator of surface lowering in accumulation areas is limited by the sample size. The rates of missing grid values in accumulations areas (Table 8; Table 9; Table 10) are high. Based on visual inspection the mode value was used as the best guess for West Qongterang Glacier and Qinbingtan Glacier No. 74 whereas assumption S1 was applied to the other sample glaciers. Longitudinal profiles were measured along Qinbingtan Glacier No. 74 in order to assess elevation changes in accumulation areas (Fig. 8). It

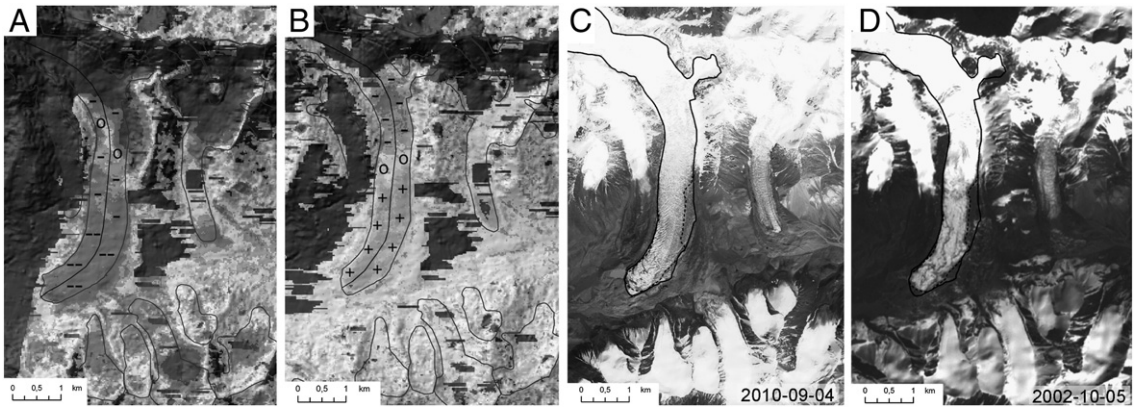

Fig. 5. A: Difference image Qinbingtan Glacier No. 74 between SPOT-5 (2009) and KH-9 Hexagon (1976), B: Difference image Qinbingtan Glacier No. 74 between SPOT-5 (2009) and SRTM3 (1999), C: SPOT-5 scene with 2002 glacier outline (dashed line) and 2010 glacier outline (solid line), D: Landsat ETM + image of Qinbingtan Glacier No. 74 indicating a glacier advance between 2002 and 2010.

is evident that, in this case, the reliability of the mode is limited to the lower accumulation area. We closed the gap in the accumulation area for the 1999–2009 period linearly and used the central value of −10 m as estimate for the average elevation change in the whole accumulation area. The bulge of the recent surge and a less distinct bulge in the 1976–2009 profile demonstrate the character of Qinbingtan Glacier No. 74 as a surging glacier.

In summary, the mass budgets of Westqongterang Glacier and Qinbingtan Glacier No. 74 are based on S2, as visual inspection and a large sample size supports the mode value as the best guess. The results of the other glaciers are based on assumption S1 as small sample sizes and a high amount of missing pixel values in accumulation areas does not allow reliable mode value calculations

The results for the Tomur Area are similar to that observed for Urumqi No. 1 considering the 1976–2009 time period (-0.35 m w.e.a^{-1} vs. -0.33 ± 0.15 m w.e.a^{-1}). However, the mass budget of Urumqi No. 1 is lower for the 1976–1999 subperiod and higher for the 1999–2009 subperiod. In comparison to Tuyuksu Glacier (Ts. Tuyuksuyskiy/Ile

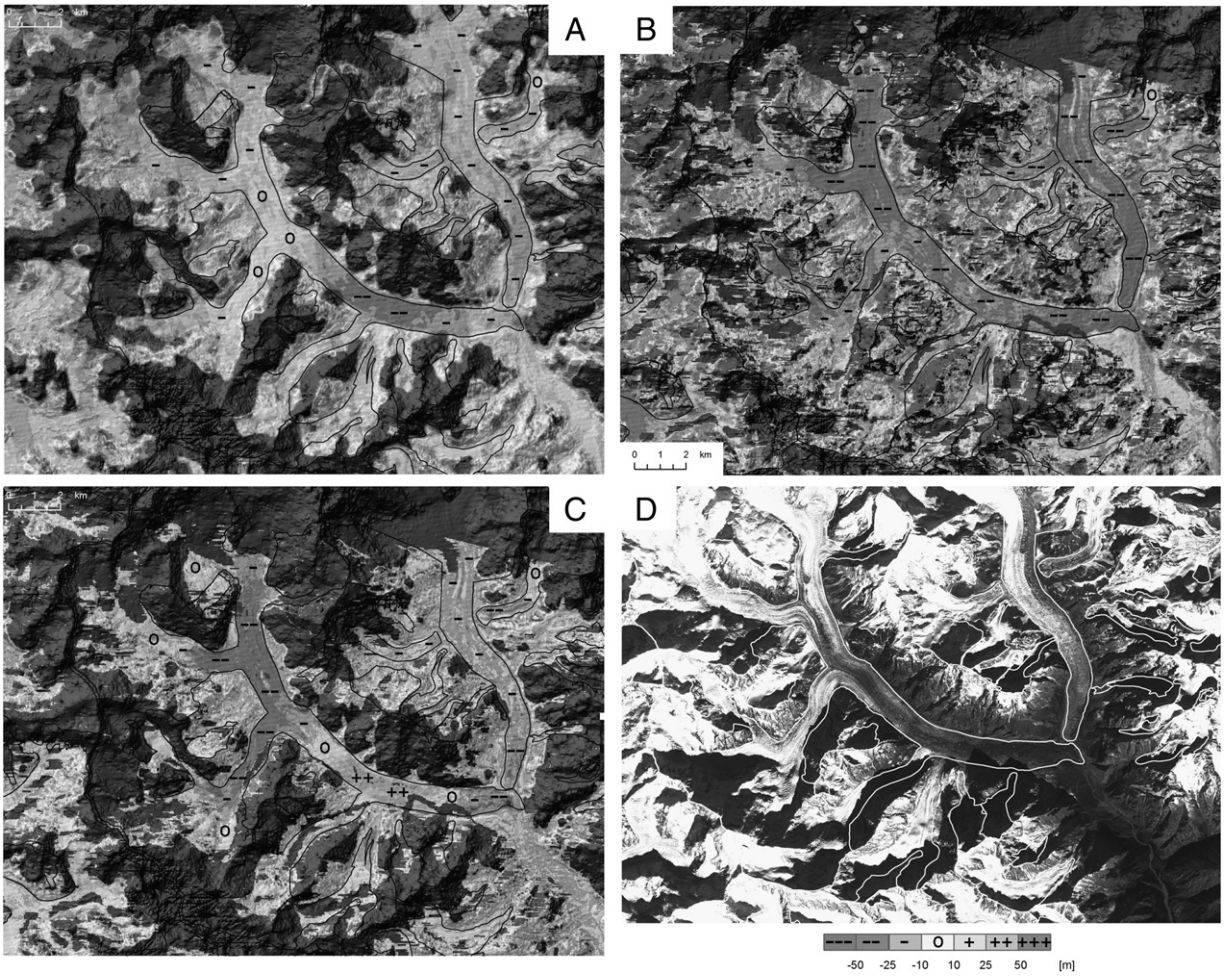

Fig. 6. A: Difference image West Qongterang Glacier between SRTM3 (1999) and KH-9 Hexagon (1976), B: Difference image West Qongterang Glacier between SPOT-5 (2009) and KH-9 Hexagon (1976), C: Difference image West Qongterang Glacier between SPOT-5 (2009) and SRTM3 (1999), D: Corresponding SPOT-5 scene.

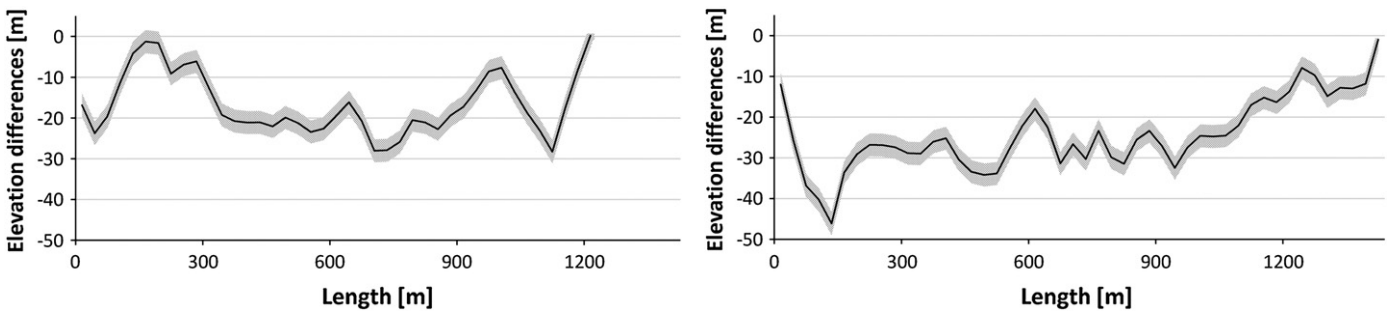

Fig. 7. Left: Profile 1 (P1) at position L1 (3170 m a.s.l.), Right: Profile 2 (P2) at position L2 (3300 m a.s.l.). The positions of P1 and P2 are identical to L1 and L2 (cf. Xie et al., 2007).

Alatau) and Karabatkak Glacier (Terskey Alatau), the other glaciers with in-situ mass balance measurements in this region (WGMS 2008), the mass budgets for the Tomur Area are significantly lower for the 1976–1999 and 1999–2009 period (Table 12).

For the Akshiirak Massif in the Central Tien Shan Aizen et al. (2007) calculated glacier elevation changes using SRTM3 data (captured in February 2000) and a DEM generated from a 1977 topographic map on a scale of 1:2500. For the 23 year time period they measured a rate of thinning of about -0.69 ± 0.37 m a^{-1}. Hence, the observed mass loss might be slightly higher but there is no significant difference in comparison to the here investigated area (-0.48 ± 0.23 m w.e.a^{-1}).

Comparing the specific glacier mass budgets for all glaciers in the study area of -0.33 ± 0.15 m w.e.a^{-1} between 1976 and 2009 and -0.23 ± 0.19 m w.e.a^{-1} between 1999 and 2009 indicates a deceleration in glacier lowering. The glacier overall mass loss can be explained in general by the increasing temperatures (Shi et al., 2007). For the Eastern Tien Shan, a raise of summer temperature and annual precipitation by about 0.38 ± 0.6 °C$(10a)^{-1}$ and 10.3 ± 3.9 mm$(10a)^{-1}$ was observed during 1959 and 2003 (Wang et al., 2009). Zhang et al. (2006) found the significant rise in air temperature as the main impact factor for the mass loss of Koxkar Glacier which surpasses the precipitation increase. The deceleration of mass loss in this region might be explained by the alteration of the local climate from warm and dry conditions to warm and wet conditions with further increase of precipitation in the recent decades as reported by Shi et al. (2007) and Zhao et al. (2011). The slight decrease of the runoff at Xehera gaging station (Yu et al., 2011) on the Kunma Like River (branch of Aksu River) and the increase of non-glacial runoff (Zhao et al., 2011) support our finding of decelerating negative glacier mass budgets in the Aksu catchment. The assumption of declining or stagnating negative glacier mass budgets is also confirmed by Toxkan River, originating in the Koshaal-Too mountain range, whose annual total runoff increased mainly due to an increase of non-glacial runoff (Zhao et al., 2011). However, further investigations about the climate–glacier interactions are required as neither a long-term meteorological station is located in the study region nor are the stations in Northwestern China located in higher elevations.

The reliability of our results is mainly influenced by the quality of the used DTMs. KH-9 Hexagon, in particular, shows the importance of a thorough analog-to-digital conversion in order to achieve sound results. Calibration inaccuracies of the used scanning device led to vertical stripping effects still visible in the difference image. Nevertheless, KH-9 Hexagon proved to be suitable in order to obtain significant glacier lowering rates for a large sample of glaciers in a highly glacierized region like the Aksu-Tarim Catchment.

7. Conclusions

The present study, dedicated to the investigation of glacier thickness changes in the Aksu-Tarim Catchment Area using KH-9 Hexagon and SPOT-5 stereo data, revealed a significant glacier surface lowering within the last three decades. The behavior of the glaciers in the study area was heterogeneous depending upon size and debris-cover. In total, the glacier mass budgets are strongly negative in the time period 1976–2009 with -0.33 ± 0.15 m w.e.a^{-1}. In the recent years a decelerated loss of -0.23 ± 0.19 m w.e.a^{-1} was measured. The highest thinning rates could be observed for the Koxkar, West Qongterang and Tomur Glacier, despite thick debris-cover. Some glaciers showed significant volume gains since 1999. Qinbingtan Glacier No. 74, in particular, shows a huge mass movement from the upper to lower part of the glacier. A positive mass balance of 0.24 ± 0.19 m w.e.a^{-1} since 1999 with a surface lowering in the accumulation area of about -10 m indicates a surging glacier.

It could be shown that KH-9 Hexagon is valuable for investigations of glacier changes since the 1970s. The sensor constellation, similar to that of the Large Format Camera, offered stereo capabilities which enables the generation of DTMs with an absolute accuracy better than

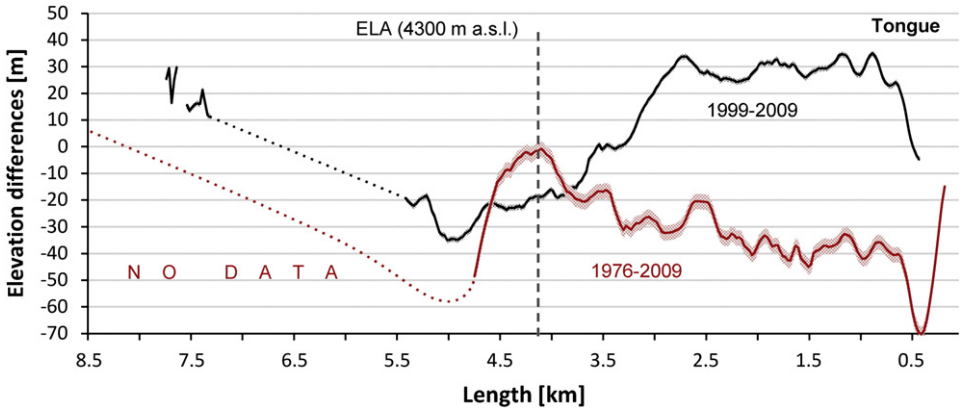

Fig. 8. Longitudinal profiles of Qinbingtan Glacier No. 74 for the 1976–2009 and 1999–2009 time period. Note that the tongue was 370 m shorter in 2009 than in 1976. The accumulation area coverage in 1976 is limited to the lower part until km 4.7.

Table 12
Glacier mass budgets of the Tomur Area in comparison to adjacent long term mass budget measurement stations in the Central Tien Shan (WGMS, 2011).

Glacier	1958–1976 (m w.e.a^{-1})	1976–1999 (m w.e.a^{-1})	1976–2009 (m w.e.a^{-1})	1999–2009 (m w.e.a^{-1})
Urumqi No. 1(43°07′, 86°48′)	−0.04	−0.26	−0.35	−0.53
Ts. Tuyuksuyskiy (43°02′, 77°04′)	−0.17	−0.54	−0.48	−0.35
Karabatkak (42°08′, 78°16′)	−0.24	−0.58 (1976–1997)		
Koxkar (41°46′, 78°16′)		−0.35 ± 0.23	−0.27 ± 0.15	−0.08 ± 0.19
Total study area		−0.48 ± 0.23	−0.33 ± 0.15	−0.23 ± 0.19

20 m in comparison to ICESat GLA14 elevation values. Debris-covered glaciers, in particular, are well represented by the DTM whereas large data gaps occurred in areas with low contrast such as snow-covered areas.

Acknowledgments

This study was conducted in the framework of the bundle project "Water Resources in the Aksu-Tarim-River Catchment of Western China and the Effects of Climate Change" (AKSU-TARIM) supported by the Deutsche Forschungsgemeinschaft (DFG, Code BO 3199/2-1) and serves as a baseline study for the project Sustainable Management of River Oases along the Tarim River/China (SuMaRiO) funded by the BMBF (Code 01 LL 0918 B). Additional support was provided by the project "Glaciers_cci" funded by the ESA (Code 4000101778/10/I-AM) and by the CAS (Chinese Academy of Sciences) project number KZCX2-YW-GJ04.

We thank ISIS-CNES for providing SPOT-5 data in the frame of the ISIS Programme. We are also grateful to the valuable comments of Juliane Peters and Manfred Buchroithner (TU Dresden) and the anonymous reviewers.

References

Aizen, V. B., Kuzmichenok, V. A., Surazakov, A. B., & Aizen, E. M. (2006). Glacier changes in the central and northern Tien Shan during the last 140 years based on surface and remote-sensing data. *Annals of Glaciology*, *43*, 202–213.

Baltsavias, E., Kocaman, S., Akca, A., & Wolff, K. (2007). Geometric and radiometric investigations of CARTOSAT-1 data. *Proc. ISPRS Workshop—High Resolution Earth Imaging for Geospatial Information, Hannover, Germany, 29 May–01 June* (13 pp. (on CDROM)).

Beaulieu, A., & Clavet, D. (2009). Accuracy assessment of Canadian digital elevation data using ICESat. *Photogrammetric Engineering and Remote Sensing*, *75*(1), 81–86.

Berthier, E., Arnaud, Y., Kumar, R., Ahmad, S., Wagnon, P., & Chevallier, P. (2007). Remote sensing estimates of glacier mass balances in the Himachal Pradesh (Western Himalaya, India). *Remote Sensing of Environment*, *108*, 327–338.

Berthier, E., & Toutin, T. (2008). SPOT5-HRS digital elevation models and the monitoring of glacier elevation changes in North-West Canada and South-East Alaska. *Remote Sensing of Environment*, *112*(5), 2443–2454.

Bhambri, R., & Bolch, T. (2009). Glacier mapping: A review with special reference to the Indian Himalayas. *Progress in Physical Geography*, *33*(5), 672–704.

Bolch, T., Kulkarni, A., Kääb, A., Huggel, C., Paul, F., Cogley, J. G., et al. (2012). The state and fate of Himalayan glaciers. *Science*, *360*(6079), 310–314.

Bolch, T., Pieczonka, T., & Benn, D. I. (2011). Multi-decadal mass loss of glaciers in the Everest area (Nepal. Himalaya). *The Cryosphere*, *5*, 349–358.

Bolch, T., Yao, Z., Kang, S., Buchroithner, M. F., Scherer, D., Maussion, F., et al. (2010). A glacier inventory for the western Nyainqentanglha Range and Nam Co Basin, Tibet, and glacier changes 1976–2009. *The Cryosphere*, *4*, 419–433.

Center for the Study of National Reconnaissance (2011). *Hexagon—America's eyes in the space.* Center for the Study of National Reconnaissance Fact Sheet.

Copland, L., Sylvestre, T., Bishop, M. P., Shroder, J. F., Seong, Y. B., Owen, L. A., et al. (2011). Expanded and recently increased glacier surging in the Karakoram. *Arctic, Antarctic, and Alpine Research*, *43*(4), 503–516.

Dolgoushin, L. D., & Osipova, G. B. (1975). *Glacier surges and the problem of their forecasting.* Moscow: Proc. Snow and Ice Symposium (13 pp.).

Falorni, G., Teles, V., Vivoni, E. R., Bras, R. L., & Amaratunga, K. S. (2005). Analysis and characterization of the vertical accuracy of digital elevation models from the Shuttle Radar Topography Mission. *Journal of Geophysical Research*, *110*(F02005), 1–20.

Fan, Y., Chen, Y., Li, W., Wang, H., & Li, X. (2011). Impacts of temperature and precipitation on runoff in the Tarim River during the past 50 years. *Journal of Arid Land*, *3*(3), 220–230.

Fisher, P. F., & Tate, N. J. (2006). Causes and consequences of error in digital elevation model. *Progress in Physical Geography*, *30*(4), 467–489.

Galiatsatos, N., Donoghue, D. N. M., & Philip, G. (2008). High resolution elevation data derived from stereoscopic CORONA imagery with minimal ground control: An approach using Ikonos and SRTM data. *Photogrammetric Engineering and Remote Sensing*, *47*(9), 1093–1106.

Gardelle, J., Berthier, E., & Arnaud, Y. (2012a). Impact of resolution and radar penetration on glacier elevation changes computed from DEM differencing. *Journal of Glaciology*, *58*(208), 419–422.

Gardelle, J., Berthier, E., & Arnaud, Y. (2012b). Slight mass gain of Karakoram glaciers in the early twenty-first century. *Nature Geoscience*, *5*, 322–325.

Gorokhovich, Y., & Voustianiouk, A. (2006). Accuracy assessment of the processed SRTM-based elevation data by CGIAR using field data from USA and Thailand and its relation to the terrain characteristics. *Remote Sensing of Environment*, *104*, 409–415.

Gruber, S. (2012). Derivation and analysis of a high-resolution estimate of global permafrost zonation. *The Cryosphere*, *6*(1), 221–233.

Harding, D. J., & Carabajal, C. C. (2005). ICESat waveform measurements of within-footprint topographic relief and vegetation vertical structure. *Geophysical Research Letters*, *32* (L21S10).

Hewitt, K. (2007). Tributary glacier surges: an exceptional concentration at Panmah Glacier, Karakoram Himalaya. *Journal of Glaciology*, *53*(181), 181–188.

Höhle, J., & Höhle, M. (2009). Accuracy assessment of digital elevation models by means of robust statistical methods. *ISPRS Journal of Photogrammetry and Remote Sensing*, *64*(4), 398–406.

Iwata, S. (2009). Mapping features of Fedchenko Glacier, the Pamirs, Central Asia from space. *Geographical Studies*, *84*, 33–43.

Kääb, A. (2008). Glacier volume changes using ASTER satellite stereo and ICESat GLAS laser altimetry, a test study on Edgeya, Eastern Svalbard. *IEEE Transactions on Geoscience and Remote Sensing*, *46*, 2823–2830.

Kääb, A. (2010). Aerial photogrammetry in glacier studies. In P. Pellikka, & W. G. Rees (Eds.), *Remote sensing of glaciers. Techniques for topographic, spatial and thematic mapping of glaciers*. (pp. 115–136) London: Taylor & Francis Group.

Kääb, A., Berthier, E., Nuth, C., Gardelle, J., & Arnaud, Y. (2012). Contrasting patterns of early twenty-first-century glacier mass change in the Himalayas. *Nature*, *488*(7412), 495–498.

Kaser, G., Grosshauser, M., & Marzeion, B. (2010). Contribution potential of glaciers to water availability in different climate regimes. *Proceedings of the National Academy of Sciences*, *107*, 20223–20227.

König, M., Winther, J. G., & Isaksson, E. (2001). Measuring snow and glacier ice properties from satellite. *Reviews of Geophysics*, *39*(1), 1–27.

Korona, J., Berthier, E., Bernard, M., Rémy, F., & Thouvenot, E. (2009). SPIRIT. SPOT 5 stereoscopic survey of polar Ice: Reference images and topographies during the fourth international polar year (2007–2009). *ISPRS Journal of Photogrammetry and Remote Sensing*, *64*, 204–212.

Kotlyakov, V., Osipova, G., & Tsvetkov, D. G. (2008). Monitoring surging glaciers of the Pamirs, central Asia, from space. *Annals of Glaciology*, *48*, 125–134.

Kutuzov, S., & Shahgedanova, M. (2009). Glacier retreat and climatic variability in the eastern Terskey–Alatoo, inner Tien Shan between the middle of the 19th century and beginning of the 21st century. *Global and Planetary Change*, *69*, 59–70.

Li, Z., Han, T., Jin, Z., Yang, H., & Jiao, K. (2003). A summary of 40-year observed variation facts of climate and Glacier No. 1 at headwater of Urumqi River, Tianshan, China. *Journal of Glaciology and Geocryology*, *25*(2), 117–123.

Liu, S., Ding, Y., Zhang, Y., Shangguan, D., Li, J., Han, H., et al. (2006). Impact of the glacial change on water resources in the Tarim River Basin. *Acta Geographica Sinica*, *61*(5), 482–490.

Magruder, L. A., Webb, C. E., Urban, T. J., Silverberg, E. C., & Schutz, B. E. (2007). ICESat altimetry data product verification at white sands space harbor. *IEEE Transactions on Geoscience and Remote Sensing*, *45*(1), 147.155.

Mao, D., Han, D., & Zhang, F. (1998). *Water resource environment and management for Talimu Basin* (pp. 37–40). Beijing: Environment Science Publishing House of China.

Miller, P. E., Kunz, M., Mills, J. P., King, M. A., Murray, T., James, T. D., & Marsh, S. H. (2009). Assessment of Glacier Volume Change Using ASTER-Based Surface Matching of Historical Photography. *IEEE Transactions of Geoscience and Remote Sensing*, *47*(7), 1971–1979.

Narama, C., Kääb, A., Duishonakunov, M., & Abdrakhmatov, K. (2010). Spatial variability of recent glacier area changes in the Tien Shan Mountains, Central Asia, using Corona (1970), Landsat (2000), and ALOS (2007) satellite data. *Global and Planetary Change*, *71*, 42–54.

Nuth, C., & Kääb, A. (2011). Co-registration and bias corrections of satellite elevation data sets for quantifying glacier thickness change. *The Cryosphere*, *5*, 271–290.

Paul, F., & Haeberli, W. (2008). Spatial variability of glacier elevation changes in the Swiss Alps obtained from two digital elevation models. *Geophysical Research Letters*, *35*, L21502.

Paul, F., Kääb, A., Maisch, M., Kellenberger, T., & Haeberli, W. (2004). Rapid disintegration of Alpine glaciers observed with satellite data. *Geophysical Research Letters*, *31*(21), L21402.

Pieczonka, T., Bolch, T., & Buchroithner, M. F. (2011). Generation and evaluation of multi-temporal digital terrain models of the Mt. Everest area from different optical sensors. *ISPRS Journal of Photogrammetry and Remote Sensing*, *66*, 927–940.

Quincey, D. J., Braun, M., Glasser, N. F., Bishop, M. P., Hewitt, K., & Luckman, A. (2011). Karakoram glacier surge dynamics. *Geophysical Research Letters*, *38*, L18504.

Reuter, H. I., Nelson, A., & Jarvis, A. (2007). An evaluation of void filling interpolation methods for SRTM data. *International Journal of Geographical Information Science*, *21*(9), 983–1008.

Rivera, A., Casassa, G., Bamber, J., & Kääb, A. (2005). Ice-elevation changes of Glaciar Chico, southern Patagonia, using ASTER DEMs, aerial photographs and GPS data. *Journal of Glaciology*, *51*(172), 105–112.

Rodriguez, E., Morris, C. S., & Belz, J. E. (2006). A global assessment of the SRTM performance. *Photogrammetric Engineering and Remote Sensing*, *72*, 249–260.

Schwitter, M. P., & Raymond, C. F. (1993). Changes in the longitudinal profiles of glaciers during advance and retreat. *Journal of Glaciology*, *39*(133), 582–590.

Shi, Y. (2008). Concise glacier inventory of China. Shanghai: Shanghai Popular Science Press.

Shi, Y., Mi, D., Yao, T., Zeng, Q., & Liu, C. (2010). Glaciers of Asia—Glaciers of China. In R. S. WilliamsJr., & J. G. Ferrigno (Eds.), *Satellite image atlas of glaciers of the world* (pp. 127–165). Denver: U.S. Geological Survey Information Services.

Shi, Y., Shen, Y., Kang, E., Li, D., Ding, Y., Zhang, G., et al. (2007). Recent and future climate change in northwest China. *Climatic Change*, *8*, 379–393.

Sorg, A., Bolch, T., Stoffel, M., Solomina, O., & Beniston, M. (2012). Climate change impacts on glaciers and runoff in Central Asia. *Nature Climate Change*, *2*, 725–731.

Surazakov, A. B., & Aizen, V. B. (2010). Positional accuracy evaluation of declassified Hexagon KH-9 mapping camera imagery. *Photogrammetric Engineering and Remote Sensing*, *76*(5), 603–608.

Tucker, C. J., Grant, D. M., & Dykstra, J. D. (2004). NASA's global orthorectified Landsat data set. *Photogrammetric Engineering and Remote Sensing*, *7*(3), 313–322.

Wang, Y., Hou, S., & Liu, Y. (2009). Glacier changes in the Karlik Shan, eastern Tien Shan, during 1971/72–2001/02. *Annals of Glaciology*, *50*(53), 39–45.

Wang, P., Li, Z., Li, H., Wang, W., & Wang, F. (2011a). Ice surface-elevation change and velocity of Qingbingtan Glacier No. 72 in the Tomor region, Tianshan Mountains, central Asia. *Journal of Mountain Science*, *8*(6), 855–864.

Wang, S., Zhang, M., Li, Z., Wang, F., Li, H., Li, Y., et al. (2011b). Response of glacier area variation to climate change in Chinese Tianshan mountains in the past 50 years. *Acta Geographica Sinica*, *66*(1), 38–46.

WGMS (2011). Glacier Mass Balance Bulletin No. 11 (2008–2009). In M. Zemp, S. U. Nussbaumer, I. Gärtner-Roer, M. Hoelzle, F. Paul, & W. Haeberli (Eds.), *Glacier Mass Balance Bulletin* (pp. 102). Zurich: ICSU (WDS)/IUGG (IACS)/UNEP/UNESCO/WMO, World Glacier Monitoring Service.

Xie, C., Ding, Y., Chen, C., & Han, T. (2007). Study on the change of Keqikaer Glacier during the last 30 years, Mt. Tuomuer, Western China. *Environmental Geology*, *51*, 1165–1170.

Xie, C., Ding, Y., Liu, S., & Chen, C. (2006). Response of meltwater runoff to air-temperature fluctuations on Keqikaer glacier, south slope of Tuomuer mountain, western China. *Annals of Glaciology*, *43*(1), 275–279.

Xu, J., Liu, S., Zhang, S., & Shangguan, D. (2006). Glaciers fluctuations in the Karamilan–Keriya River watershed in the past 30 years. *Journal of Glaciology and Geocryology*, *28*(3), 312–318.

Yu, P., Xu, H., Liu, S., An, H., Zhang, Q., & Gong, J. (2011). The nonlinear characteristics of annual runoff change in Aksu River. *Journal of Natural Resources*, *26*(8), 1412–1422.

Zhang, Y., Liu, S., Ding, Y., Li, Y., & Shangguan, D. (2006). Preliminary study of mass balance on the Keqicar Baxi Glacier on the south slopes of Tianshan mountains. *Journal of Glaciology and Geocryology*, *28*(4), 477–484.

Zhao, Q., Ye, B., Ding, Y., Zhang, S., Zhao, C., Wang, J., et al. (2011). Simulation and analysis of river runoff in typical cold regions. *Sciences in Cold and Arid Regions*, *3*(6), 0498–0508.

Zhou, C., Yang, W., Wu, L., & Liu, S. (2009). Glacier changes from a new inventory, Nianchu river basin, Tibetan Plateau. *Annals of Glaciology*, *50*(53), 87–92.